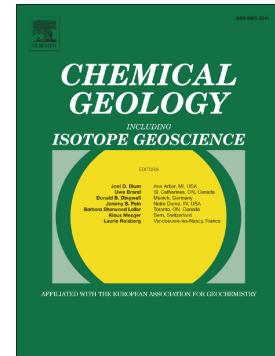


Accepted Manuscript

Mercury stable isotope compositions of Chinese urban fine particulates in winter haze days: Implications for Hg sources and transformations

H.M. Xu, R.Y. Sun, J.J. Cao, Ru-Jin Huang, B. Guinot, Z.X. Shen, M. Jiskra, C.X. Li, B.Y. Du, C. He, S.X. Liu, T. Zhang, J.E. Sonke



PII: S0009-2541(18)30579-5
DOI: <https://doi.org/10.1016/j.chemgeo.2018.11.018>
Reference: CHEMGE 18980
To appear in: *Chemical Geology*
Received date: 4 June 2018
Revised date: 1 November 2018
Accepted date: 25 November 2018

Please cite this article as: H.M. Xu, R.Y. Sun, J.J. Cao, Ru-Jin Huang, B. Guinot, Z.X. Shen, M. Jiskra, C.X. Li, B.Y. Du, C. He, S.X. Liu, T. Zhang, J.E. Sonke, Mercury stable isotope compositions of Chinese urban fine particulates in winter haze days: Implications for Hg sources and transformations. *Chemge* (2018), <https://doi.org/10.1016/j.chemgeo.2018.11.018>

This is a PDF file of an unedited manuscript that has been accepted for publication. As a service to our customers we are providing this early version of the manuscript. The manuscript will undergo copyediting, typesetting, and review of the resulting proof before it is published in its final form. Please note that during the production process errors may be discovered which could affect the content, and all legal disclaimers that apply to the journal pertain.

Mercury stable isotope compositions of Chinese urban fine particulates in winter haze days: implications for Hg sources and transformations

H.M. Xu^{1,3,4}, R.Y. Sun^{2*}, J.J. Cao^{3*}, Ru-Jin Huang³, B. Guinot⁴, Z.X. Shen¹, M. Jiskra⁵, C.X. Li^{5,6}, B.Y. Du⁷, C. He¹, S.X. Liu³, T. Zhang³, J. E. Sonke⁵

¹ Department of Environmental Science and Engineering, Xi'an Jiaotong University, Xi'an, China

² Institute of Surface-Earth System Science, Tianjin University, Tianjin, China

³ SKLLQG, Key Lab of Aerosol Chemistry & Physics, Institute of Earth Environment, Chinese Academy of Sciences, Xi'an, China

⁴ Laboratoire d'Aérodologie, Université de Toulouse, CNRS, UPS, France

⁵ Observatoire Midi-Pyrénées, Laboratoire Géosciences Environnement Toulouse, CNRS/IRD/Université de Toulouse, France

⁶ EcoLab Université de Toulouse, CNRS, INPT, UPS, Castanet Tolosan, France

⁷ State Key Laboratory of Environmental Geochemistry, Institute of Geochemistry, Chinese Academy of Sciences, Guiyang, China

*Corresponding authors: R. Y. Sun (ruoyu.sun@tju.edu.cn)

J.J. Cao (cao@loess.llqg.ac.cn)

Abstract

Atmospheric pollution by fine particulates and mercury (Hg) in emerging economies is a serious environmental concern. Here, we present Hg concentrations and isotope compositions of 24-hour integrated fine particulate matter (PM_{2.5}) samples collected during January, 2014 at four large Chinese cities (three inland cities: Beijing, Changchun and Chengdu; one coastal city: Hong Kong), with an aim of identifying the potential Hg sources and transformation processes. Mean concentrations of PM_{2.5} (171±62 μg m⁻³) and PM_{2.5}-bound Hg (1.3±1.1 ng m⁻³) in Chengdu were the highest. Overall, PM_{2.5} samples in Chinese inland cities were characterized by moderately negative δ²⁰²Hg (-1.08±0.64‰, 1σ), slightly negative Δ¹⁹⁹Hg (-0.13±0.28‰, 1σ) and insignificant Δ²⁰⁰Hg (0.03±0.05‰, 1σ). On average, δ²⁰²Hg of PM_{2.5} was the highest in Chengdu (-0.74±0.67‰, 1σ), followed by Beijing (-1.11±0.26‰, 1σ) and Changchun (-1.60±0.45‰, 1σ). PM_{2.5} from Beijing showed the most negative Δ¹⁹⁹Hg (-0.31±0.40‰, 1σ) that was significantly lower than Changchun (-0.12±0.21‰, 1σ) and Chengdu (-0.02±0.15‰, 1σ). Coal combustion and cement production were identified to be the dominant sources of PM_{2.5}-bound Hg in these cities, with additional Hg sources from non-ferrous metal smelting in Chengdu. Besides, Hg emissions from biomass burning were evident in specific days for each city. We found that source materials and isotope fractionation during emission processes could not fully explain the observed Hg isotope compositions in PM_{2.5}, especially the large negative Δ¹⁹⁹Hg values (<-0.3‰) in Beijing. The near-unity slope of Δ¹⁹⁹Hg vs. Δ²⁰¹Hg in PM_{2.5} samples from each studied city indicates that Hg^{II} in the fine aerosols was likely photo-reduced to different degrees in the atmosphere following emission from sources.

Keywords: PM_{2.5}; mercury isotope; Chinese cities; Hg source; photoreduction

1. Introduction

Countries with emerging economies (e.g. China and India) have been experiencing the most serious atmospheric particulate pollution since the last two decades (Huang et al., 2014). The fine particulates, such as PM_{2.5} (aerodynamic equivalent diameter equal to or less than 2.5 μm), are of particular interests because they can easily penetrate into the respiratory systems of human beings, causing adverse health effects (Cao et al., 2012; Dockery & Pope, 1996). In addition, PM_{2.5} is an effective vector of various toxic elements such as mercury (Hg) and lead (Pb), constituting an important pathway of toxic metal exposure (USEPA, 2006; WHO, 2007).

Hg is a neuro-toxic element with an atmospheric residence time of ~6 months, enabling its hemispheric and global transport (Horowitz et al., 2017). Three operationally defined Hg species exist in the atmosphere: gaseous elemental Hg (GEM), gaseous oxidized Hg^{II} (GOM) and particulate-bound Hg^{II} (PBM). GEM generally accounts >90% of the total atmospheric Hg, and the GOM and PBM, while at sites close to pollution sources, can represent up to 10% (Fu et al., 2015). GEM is relatively inert, but can be converted to GOM and PBM which are readily removed by atmospheric wet and dry deposition within several weeks (Driscoll et al., 2013; Selin et al., 2007). On the other hand, PBM in which Hg^{II} binds to dissolved organic carbon or organic ligands in aqueous aerosols is postulated to be photo-reduced back into GEM (Horowitz et al., 2017). Thus, the levels of PBM are not only affected directly by the particulate emission sources, but also by the competing Hg redox chemistry in the atmosphere. The PBM concentration in the atmosphere is generally below 0.1 ng m⁻³ in the background environment, and may reach several ng m⁻³ in the urban-industrial areas (Fu et al., 2015; Gustin et al., 2015).

Elucidating the factors that govern the levels of PBM, especially Hg bound to fine particulates like PM_{2.5} (PM_{2.5}-bound Hg) is equally important for mitigating PM_{2.5} and Hg pollution (Huang et al., 2016; Huang et al., 2015; Xu et al., 2017b; Yu et al., 2016). Hg stable isotope composition has become a new tool to study the sources and processes

of Hg in various environmental compartments (Blum et al., 2014; Sonke and Blum, 2013; Yin et al., 2014b). Hg isotopes can be fractionated mass-dependently (MDF) by nearly all biogeochemical processes. Mass-independent fractionation (MIF) of Hg isotopes primarily occurs during photochemical reactions (Bergquist and Blum, 2007; Sun et al., 2016a). This results in the variations of at least three useful isotope signatures ($\delta^{202}\text{Hg}$, $\Delta^{199}\text{Hg}$ and $\Delta^{200}\text{Hg}$, representing MDF, odd isotope MIF and even isotope MIF, respectively). Measurement of these Hg isotope signatures has been successfully applied to trace the potential Hg pollution sources and biogeochemical processes that Hg undergoes in the atmosphere (Huang et al., 2016; Xu et al., 2017b).

Recently, Hg isotope compositions have been reported for different atmospheric Hg species. In general, atmospheric gaseous Hg (mainly GEM) shows slightly positive $\delta^{202}\text{Hg}$ ($0.10 \pm 0.65\%$, 1σ , $n=221$), and slightly negative $\Delta^{199}\text{Hg}$ ($-0.11 \pm 0.12\%$, 1σ , $n=221$) and $\Delta^{200}\text{Hg}$ ($-0.04 \pm 0.05\%$, 1σ , $n=221$) (Demers et al., 2013; Demers et al., 2015; Enrico et al., 2016; Fu et al., 2016a; Gratz et al., 2010; Sherman et al., 2010; Xu et al., 2017b; Yu et al., 2016), which are complementary to wet precipitation (rain and snow,) showing negative $\delta^{202}\text{Hg}$ ($-0.81 \pm 0.57\%$, 1σ , $n=163$), and positive $\Delta^{199}\text{Hg}$ ($0.39 \pm 0.31\%$, 1σ , $n=163$) and $\Delta^{200}\text{Hg}$ ($0.20 \pm 0.20\%$, 1σ , $n=163$) (Chen et al., 2012; Demers et al., 2013; Donovan et al., 2013; Enrico et al., 2016; Gratz et al., 2010; Sherman et al., 2015; Sherman et al., 2012; Wang et al., 2015; Yuan et al., 2015). Hg isotope compositions of atmospheric particulates have been measured in total suspended particulates (TSP) and $\text{PM}_{2.5}$ from several major cities of China (Beijing, Guiyang, Xi'an) (Huang et al., 2016; Huang et al., 2015; Xu et al., 2017b; Yu et al., 2016), and in PM_{10} from Kolkata, eastern India (Das et al., 2016). They are characterized by negative $\delta^{202}\text{Hg}$ ($-1.01 \pm 0.76\%$, 1σ) and very small MIF ($\Delta^{199}\text{Hg} = -0.01 \pm 0.15\%$; $\Delta^{200}\text{Hg} = 0.03 \pm 0.04\%$, 1σ) (Huang et al., 2016; Huang et al., 2015; Xu et al., 2017b; Yu et al., 2016). The above observations highlight the potential of using Hg isotope signatures to anchor PBM emission sources, but stress that the complex atmospheric Hg isotope fractionation processes might obscure the Hg source-receptor relationship.

In this study, we simultaneously collected $\text{PM}_{2.5}$ samples in three Chinese inland

cities (Beijing, Changchun and Chengdu) that suffer from serious haze pollution, and in one coastal city Hong Kong. Sampling was mainly conducted in January 2014 when the haze pollution events were the most frequent. Our objectives are to: 1) characterize the Hg isotope variation ranges in urban atmospheric fine particulates over a large spatial scale, 2) identify the dominant anthropogenic Hg sources in different Chinese cities, and 3) illustrate if the source Hg isotope compositions of fine particulates were shifted by the emission and post-emission processes during the aerosol formation.

2. Materials and Methods

2.1. Site description

Four cities were chosen for PM_{2.5} sampling: Beijing and Changchun in northern China, Chengdu in southern China, and Hong Kong as a reference site (Figure S1). The sampling period for each city lasted for ~30 days, spanning from the end of December 2013 to the end of January 2014 (0-2 days before the Chinese New Year or Chinese Spring Festival in 31 January 2014) when the haze pollution was most severe in mainland China.

Beijing, the capital of China, is one of the world's most populous cities with a population of over 20 million in an area of 16,410 km². It is located in a basin with a typical continental monsoon climate. PM_{2.5} was sampled from 30 December 2013 to 31 January 2014 (the sample collected in 26 January was invalid and discarded) on the roof (8 m above the ground level, 65 m away from the urban road) of an experimental building in the Tower Division of the Institute of Atmospheric Physics, Chinese Academy of Sciences (N 39.59°, E 116.22°).

Changchun, the capital city of Jilin province is an industrial city, with a population of ~8 million in an area of 20,565 km². It is situated on a flat plain, with a typical continental monsoon climate. The winter is cold and dry, and lasts from November to March. PM_{2.5} was sampled from 30 December 2013 to 30 January 2014 on a platform (1.5 m above the ground level, 130 m away from the urban road) in the Changchun

Meteorological Bureau (N 43.54°, E 125.13°).

Chengdu, the capital city of Sichuan province, is located at the western edge of the Sichuan Basin, with a population of over 14 million in an area of 14,312 km². It has a humid, subtropical climate and a very low annual sunshine time of ~1000 hours. PM_{2.5} was sampled from 30 December 2013 to 28 January 2014 on a platform (1.5 m above the ground level, 270 m away from the urban road) in the Institute of Plateau Meteorology, China Meteorological Administration (N 30.39°, E 104.00°).

Hong Kong, an autonomous territory on the southern coast of China, is one of the world's most densely populated cities, with a population of over 7 million in a small area of 1104 km². Hong Kong is located in the Pearl River Delta region, and has a humid, subtropical climate, with an annual average sunshine time of ~2000 hours. PM_{2.5} was sampled from 30 December 2013 to 28 January 2014 on a platform (1.5 m above the ground level, 2 m away from the urban road) beside the Hong Kong Polytechnic University (N 22.18°, E 114.10°).

The meteorological parameters including temperature, sunlight time, dew-point, relative humidity (RH), pressure, visibility, and wind speed (binned and averaged daily) during the sampling periods were obtained from the meteorological bureau of each city (Table S1). AQI (Air Quality Index), CO, SO₂, NO₂, O₃ in Beijing, Changchun and Chengdu were retrieved from the Real-time Monitoring Platform of Chinese Air Quality (<https://www.aqistudy.cn/>).

2.2. Sampling of PM_{2.5}

Each PM_{2.5} sample was collected on a pre-baked (780 °C, 3 hours) 8×10 inch quartz-fiber filter (Whatman QM-A, pore size of 2.2 μm with efficiency of >99.995% for particles 0.3 μm or larger) using a high-volume aerosol sampler with a cut-off size of 2.5 μm (TE-6070 MFC, Tisch Environmental, USA). The sampling time is approximately 24-hour at a flow rate of 1.05 m³ min⁻¹. At each sampling site, one field filter blank was also deployed. Each filter was conditioned before and after sampling in a chamber maintained at a temperature of 20-23°C and a RH of 35%-45% for 24

hours, and then was measured gravimetrically using a Sartorius LA130 S-F electronic microbalance (sensitivity: ± 0.10 mg, Sartorius, Gottingen, Germany) to calculate the mass of PM_{2.5}. The samples and field blanks were air-tightly sealed and stored in a refrigerator at -20 °C before analysis.

2.3. Concentration analysis of Hg and other species

Total Hg concentration was measured by combusting several punches (0.5 cm² per punch) of each filter in a Milestone DMA-80 Hg analyzer or Advanced Mercury AMA-254 Hg analyzer (Milestone Srl., Italy) at the Laboratoire Géosciences Environnement, Toulouse, France. Both DMA-80 and AMA-254 use an atomic absorption spectrometer to determine total mercury concentrations in samples without sample pre-treatment. The samples were first decomposed in the combustion tube with releasing interfering impurities (e.g. ash, moisture, halogens) removed in the catalyst tube. Following decomposition, the purified gas is transported to the amalgamator where Hg vapor is amalgamated with gold and then heated for subsequent detection. The detection limit is 0.1 ng for DMA-80 Hg, and 0.01 ng for AMA-254. The periodically combusted NIST-2632d coal standard gave an average Hg concentration of 97.0 ± 7.9 ng g⁻¹ (1σ , n=16), which is consistent with the certified value (92.8 ± 3.3 ng g⁻¹). The filter blanks only contained negligible Hg (0.02 ng, n=4) relative to the sample filters (1.75 ng, n=124).

Randomly selected PM_{2.5} filters from each city were also analyzed for 13 other elements (S, Cl, K, Ca, Ti, V, Cr, Mn, Fe, Co, Cu, Zn, Pb) by Energy Dispersive X-ray Fluorescence spectrometry (EDXRF) (PANalytical Epsilon 5, the Netherlands) at the Institute of Earth Environment, Chinese Academy of Sciences, Xi'an, China, according to the method described in Xu et al. (2012, 2016, 2017a). A portion of each filter was placed in a 15 mL vial containing 10 mL Milli-Q H₂O to extract the water-soluble potassium ion (K⁺). The vials were placed in an ultrasonic water bath and shaken with a mechanical shaker for 1 h. The extracts were then filtered through 0.45 μ m pore size microporous membranes before K⁺ concentration measurement in a Dionex-600 Ion

Chromatograph (Dionex Inc., Sunnyvale, CA, USA). Data reported are corrected by the field blanks. Quality assurance/quality control (QA/QC) procedures are as described by Zhang et al. (2011).

2.4. Hg stable isotope analysis

Due to limited mass and low Hg concentrations in PM_{2.5} samples from Hong Kong, they were not measured for Hg isotope compositions. PM_{2.5} samples from other three cities (Beijing, Changchun and Chengdu) were digested by 6 mL acid mixture (volumetric ratio of 3:1:2 for 15 M bi-distilled HNO₃:10 M bi-distilled HCl:Milli-Q H₂O) in closed Teflon vessels on a hot plate kept at 120 °C for at least 6 hours. Each of the digested sample solutions was then passed through a plastic syringe interfaced filter (0.22 µm, Millipore, mixed ester of cellulose nitrate and cellulose acetate). The filtered sample solution was further purified through a purge-trap setup (see supplementary information). Standard reference material NIST1944 was also processed in the same way as the samples by the purge-trap setup.

Aliquots of the treated sample solutions were measured for Hg concentrations by a cold-vapor atomic fluorescence spectroscopy (Brooks Rand Model III) to calculate Hg recovery during digestion, purification and trapping. The calculated Hg recovery was 101±19% (1σ), with a typical variation range between 80% and 120%. Hg isotope ratios were analyzed by a cold vapor multi-collector inductively coupled plasma mass spectrometry (MC-ICP-MS, Thermo-Finnigan Neptune) following the published protocols at the Laboratoire Géosciences Environnement Toulouse, France (Sun et al., 2013a). Briefly, an on-line cold vapor generator (CETAC HGX-200) was used to reduce Hg^{II} in the trapping solutions into Hg⁰ vapor by SnCl₂ solution (3%, w/v, in 1 M HCl). NIST 3133 Hg standard and in-house ETH Fluka Hg standard were matched to the Hg concentration (~1 ng g⁻¹) and matrix (~20% reverse aqua regia) of the sample solutions within 10%.

Hg isotopic ratio is reported in delta notation (δ) in unit of per mil (‰) by referencing to the bracketed NIST 3133 Hg standard:

$$\delta^{xxx}\text{Hg} = \left(\frac{\frac{xxx}{198}\text{Hg}_{\text{sample}}}{\frac{xxx}{198}\text{Hg}_{\text{NIST 3133}}} - 1 \right) \quad (1)$$

where ‘xxx’ refers to the mass numbers of measured isotopes: 199, 200, 201, 202 and 204. MIF is reported in capital delta (Δ) notation (‰), which is defined as the difference between the measured $\delta^{199}\text{Hg}$, $\delta^{200}\text{Hg}$, $\delta^{201}\text{Hg}$ and $\delta^{202}\text{Hg}$ and those predicted from $\delta^{202}\text{Hg}$ using the kinetic MDF law:

$$\Delta^{xxx}\text{Hg} = \delta^{xxx}\text{Hg} - \beta_{xxx} \times \delta^{202}\text{Hg} \quad (2)$$

where the mass-dependent scaling factor β_{xxx} is 0.252 for ^{199}Hg , 0.502 for ^{200}Hg , 0.752 for ^{201}Hg and 1.493 for ^{204}Hg . The long-term uncertainty was evaluated by repeated measurement of ETH Fluka Hg standard, which yielded a value of $-1.44 \pm 0.10\%$, $0.08 \pm 0.06\%$, $0.03 \pm 0.04\%$, $0.00 \pm 0.04\%$, $-0.02 \pm 0.18\%$ (2σ , $n=10$) for $\delta^{202}\text{Hg}$, $\Delta^{199}\text{Hg}$, $\Delta^{200}\text{Hg}$, $\Delta^{201}\text{Hg}$ and $\Delta^{204}\text{Hg}$, respectively, in agreement with the published values (Jiskra et al., 2015; Smith et al., 2015). The mean Hg isotope composition of the procedural standard NIST1944 ($-0.65 \pm 0.01\%$ for $\delta^{202}\text{Hg}$, $0.02 \pm 0.10\%$ for $\Delta^{199}\text{Hg}$, $0.02 \pm 0.05\%$ for $\Delta^{200}\text{Hg}$, $0.00 \pm 0.02\%$ for $\Delta^{201}\text{Hg}$ and $0.09 \pm 0.01\%$ for $\Delta^{204}\text{Hg}$, 2σ , $n=2$) was also in consistent with the previously reported value (Sonke et al., 2010). The 2σ uncertainties of isotope compositions for ETH Fluka were taken as the typical analytic uncertainties of isotope compositions for samples. If the 2σ uncertainties of isotope compositions for samples with multiple measurements were larger than the typical 2σ uncertainties, then the 2σ uncertainties of samples applied.

3. Results and Discussion

3.1. Spatial variations Hg concentrations and Hg isotope compositions of $\text{PM}_{2.5}$

The concentrations of $\text{PM}_{2.5}$ and $\text{PM}_{2.5}$ -bound Hg ($\text{Hg}_{\text{PM}_{2.5}}$), and Hg isotope compositions of $\text{PM}_{2.5}$ for each city are listed in Tables S2-S3, and their descriptive statistics are listed in Table 1. The mean volumetric concentration of $\text{PM}_{2.5}$ was the highest in Chengdu ($172 \pm 62 \mu\text{g m}^{-3}$, 1σ , $n=30$, 85 to $325 \mu\text{g m}^{-3}$), followed by Changchun ($126 \pm 43 \mu\text{g m}^{-3}$, 1σ , $n=32$, 74 to $279 \mu\text{g m}^{-3}$) and Beijing ($108 \pm 64 \mu\text{g m}^{-3}$,

1 σ , n=32, ranging from 28 to 319 $\mu\text{g m}^{-3}$) (Figure 1 and Table 1). The lowest mean PM_{2.5} concentration was observed in Hong Kong (88 \pm 39 $\mu\text{g m}^{-3}$, 1 σ , n=30, 45 to 217 $\mu\text{g m}^{-3}$) (Table 1). On a daily basis, 69%, 94%, 100% and 50% of the sampling days in Beijing, Changchun, Chengdu and Hong Kong, respectively, exceeded the threshold value (75 $\mu\text{g m}^{-3}$) of 24-hour PM_{2.5} concentration set by Ambient Air Quality Standard (AAQS) of China (Cao et al., 2013; GB3095-2012, 2012) (Figure 1). It is surprising that half of the sampling days in Hong Kong, known for its good air quality, had PM_{2.5} concentrations higher than the threshold value of AAQS in this study. We speculate that the high PM_{2.5} concentrations in Hong Kong might be caused by diffused pollution plumes from mainland China, because the predominate wind direction in Hong Kong during the sampling days was from the northeast mainland China (Ho et al., 2003; Jahn et al., 2011).

Table 1. Means ($\pm 1\sigma$) and ranges of PM_{2.5}, Hg_{PM2.5}, Hg enrichment factor (EF_{Hg}) and Hg isotopic compositions of PM_{2.5} in studied four Chinese cities.

	Beijing	Changchun	Chengdu	Hong Kong
PM_{2.5} ($\mu\text{g m}^{-3}$)	108.4 \pm 63.9	125.8 \pm 42.9	171.5 \pm 62.0	87.8 \pm 39.1
Range ($\mu\text{g m}^{-3}$)	27.6~319.0	74.1~279.2	85.1~324.8	44.5~217.1
Hg_{PM2.5} (ng m^{-3})	0.24 \pm 0.18	0.24 \pm 0.15	1.30 \pm 1.09	0.06 \pm 0.04
Range (ng m^{-3})	0.02~0.82	0.06~0.73	0.24~5.02	0.02~0.14
Hg_{PM2.5} ($\mu\text{g g}^{-1}$)	2.11 \pm 1.12	1.94 \pm 1.19	8.16 \pm 6.58	0.67 \pm 0.25
Range (ng m^{-3})	0.68-6.38	0.68-6.22	1.57-22.52	0.35-1.42
EF_{Hg}	252 \pm 192	158 \pm 109	1330 \pm 1066	115 \pm 51
Range	32~565	48~365	137~3302	54~197
$\delta^{202}\text{Hg}$ (‰)	-1.11 \pm 0.26	-1.60 \pm 0.45	-0.74 \pm 0.67	-
Range (‰)	-1.56~-0.71	-2.46~-0.65	-1.75~1.07	-
$\Delta^{199}\text{Hg}$ (‰)	-0.31 \pm 0.40	-0.12 \pm 0.21	-0.02 \pm 0.15	-
Range (‰)	-1.12~-0.37	-0.54~-0.21	-0.45~-0.15	-
$\Delta^{200}\text{Hg}$ (‰)	0.02 \pm 0.03	0.03 \pm 0.07	0.03 \pm 0.04	-
Range (‰)	-0.03~-0.07	-0.06~-0.14	-0.03~-0.11	-

$\Delta^{201}\text{Hg}$ (‰)	-0.35 ± 0.40	-0.17 ± 0.20	-0.11 ± 0.14	-
Range (‰)	$-1.17\sim -0.19$	$-0.54\sim -0.09$	$-0.47\sim -0.10$	-
$\Delta^{204}\text{Hg}$ (‰)	-0.02 ± 0.14	-0.09 ± 0.19	-0.02 ± 0.09	-
Range (‰)	$-0.23\sim -0.22$	$-0.50\sim -0.14$	$-0.16\sim -0.21$	-

-: not applicable

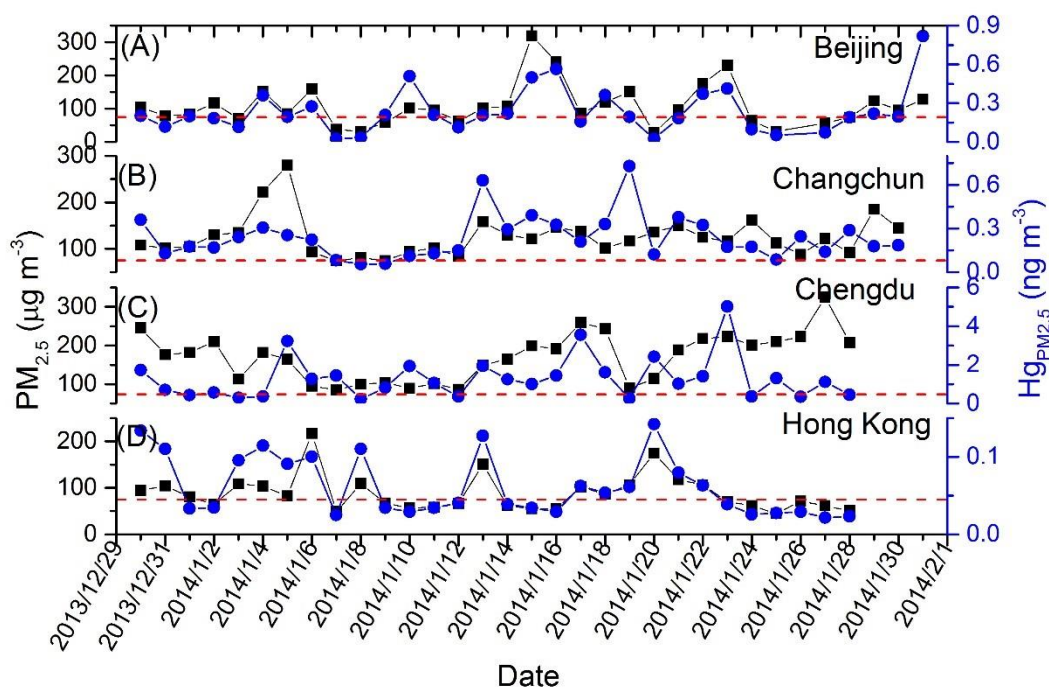


Figure 1. Temporal variations of volumetric concentrations of $\text{PM}_{2.5}$ ($\mu\text{g m}^{-3}$) and $\text{Hg}_{\text{PM}_{2.5}}$ (ng m^{-3}) in Beijing (A), Changchun (B), Chengdu (C) and Hong Kong (D). The horizontal red dashed lines indicate the threshold value of 24-hour $\text{PM}_{2.5}$ concentration ($75 \mu\text{g m}^{-3}$) in Ambient Air Quality Standard (AAQS) of China.

The mean volumetric concentration of $\text{Hg}_{\text{PM}_{2.5}}$ was also the highest in Chengdu ($1.30\pm 1.09 \text{ ng m}^{-3}$, 1σ , $n=30$, 0.24 to 5.02 ng m^{-3}), which is about one order of magnitude higher than that in Changchun ($0.24\pm 0.15 \text{ ng m}^{-3}$, 1σ , $n=32$, 0.06 to 0.73 ng m^{-3}) and Beijing ($0.24\pm 0.18 \text{ ng m}^{-3}$, 1σ , $n=32$, 0.02 to 0.82 ng m^{-3}), and is two orders of magnitude higher than that in Hong Kong ($0.06\pm 0.04 \text{ ng m}^{-3}$, 1σ , $n=30$, 0.02 to 0.14 ng m^{-3}) (Table 1). The mass concentration of $\text{Hg}_{\text{PM}_{2.5}}$ was extremely high in Chengdu ($8.16\pm 6.58 \mu\text{g g}^{-1}$, 1σ , $n=30$, 1.57 to $22.52 \mu\text{g g}^{-1}$), compared to Changchun ($1.94\pm 1.19 \mu\text{g g}^{-1}$, 1σ , $n=32$, 0.68 to $6.22 \mu\text{g g}^{-1}$), Beijing ($2.11\pm 1.12 \mu\text{g g}^{-1}$, 1σ , $n=32$, 0.68 to $6.38 \mu\text{g g}^{-1}$) and

Hong Kong ($0.67 \pm 0.25 \mu\text{g g}^{-1}$, 1σ , $n=30$, 0.35 to $1.42 \mu\text{g g}^{-1}$) (Table 1). Both regional Hg emission budgets and climate conditions could contribute to the highest $\text{Hg}_{\text{PM}_{2.5}}$ concentration in Chengdu. The provincial Hg emission budget was nearly 20 Mg yr^{-1} for Chengdu, but was less than 10 Mg yr^{-1} for other cities (Zhang et al., 2015). Among these cities, Chengdu has the highest relative humidity (69% vs. 37-58%), but lowest sunlight time (98 h vs. 192-198 h) and wind speed (4 km h^{-1} vs. $10\text{-}16 \text{ km h}^{-1}$) (Table S1) because it is located in the poorly ventilated Sichuan Basin. Amos et al. (2012) found that Hg^{II} gas-particle partitioning would be enhanced with the decrease in temperature rather than with the variation in relative humidity (RH) after examining a large set of measured data. Here, neither temperature nor relative humidity showed significant correlations with $\text{Hg}_{\text{PM}_{2.5}}$ concentration. In contrast, the wind speed showed a significantly negative correlation with $\text{Hg}_{\text{PM}_{2.5}}$ concentration ($R^2=0.89$, $p<0.01$, $n=4$). This suggests that the unfavorable air diffusion condition of Sichuan Basin possibly enhances the Hg^{II} gas-particle partitioning during aerosol formation.

The volumetric concentrations between $\text{PM}_{2.5}$ and $\text{Hg}_{\text{PM}_{2.5}}$ are positively correlated in Beijing ($R^2=0.49$, $p<0.01$, $n=32$) and Hong Kong ($R^2=0.61$, $p<0.01$, $n=30$) (Figure S2), in contrast to Changchun ($R^2=0.06$, $p>0.05$, $n=32$) and Chengdu ($R^2=0.05$, $p>0.05$, $n=30$) where no significant correlations were observed. This likely indicates that the sources of $\text{PM}_{2.5}$ in Changchun and Chengdu were more diverse than Beijing and Hong Kong, with each source containing quite different Hg levels. This is supported by the variation coefficients ($\text{VC}=\text{SD}/\text{Mean}$) of $\text{Hg}_{\text{PM}_{2.5}}$ mass concentration: Hong Kong (38%) and Beijing (53%) are lower than those of Changchun (61%) and Chengdu (81%). It is also possible that the atmospheric Hg transformation processes (e.g. GEM oxidation to GOM/PBM and GOM partitioning to PBM) are more complex in Changchun and Chengdu, which deteriorate the correlation between $\text{PM}_{2.5}$ and $\text{Hg}_{\text{PM}_{2.5}}$ that would be expected if Hg transformation processes were limited.

The collected $\text{PM}_{2.5}$ samples showed large variation in Hg isotope compositions, varying from -2.46‰ to 1.07‰ for $\delta^{202}\text{Hg}$ and -1.12‰ to 0.37‰ for $\Delta^{199}\text{Hg}$ (Figure 2). These values basically overlap the Hg isotope variation ranges (-3.48‰ to 0.51‰ for

$\delta^{202}\text{Hg}$; -0.53% to 0.57% for $\Delta^{199}\text{Hg}$) of atmospheric particulates collected from other Chinese cities (e.g. Xi'an, Guiyang) (Huang et al., 2016; Huang et al., 2015; Xu et al., 2017b; Yu et al., 2016) and Kolkata of India (Das et al., 2016) (Figure 3). The mean $\delta^{202}\text{Hg}$ value in $\text{PM}_{2.5}$ increased significantly ($p < 0.01$, one-way ANOVA) from Changchun ($-1.60 \pm 0.45\%$, 1σ , $n=18$, -2.46% to -0.65%) to Beijing ($-1.11 \pm 0.26\%$, 1σ , $n=17$, -1.56% to -0.71%) and Chengdu ($-0.74 \pm 0.67\%$, 1σ , $n=29$, -1.75% to 1.07%) (Table 1). The variation trend of $\Delta^{199}\text{Hg}$ was decoupled from that of $\delta^{202}\text{Hg}$, increasing in the order of Beijing ($-0.31 \pm 0.40\%$, 1σ , $n=17$, -1.12% to 0.37%), Changchun ($-0.12 \pm 0.21\%$, 1σ , $n=18$, -0.54% to 0.21%) and Chengdu ($-0.02 \pm 0.15\%$, 1σ , $n=29$, -0.45% to 0.15%) (Table 1). It is interesting to note that several $\text{PM}_{2.5}$ samples from Beijing had very low $\Delta^{199}\text{Hg}$ values, down to -1.1% , and $\text{PM}_{2.5}$ samples from Chengdu had the highest $\delta^{202}\text{Hg}$ and $\Delta^{199}\text{Hg}$ values (Figure 4).

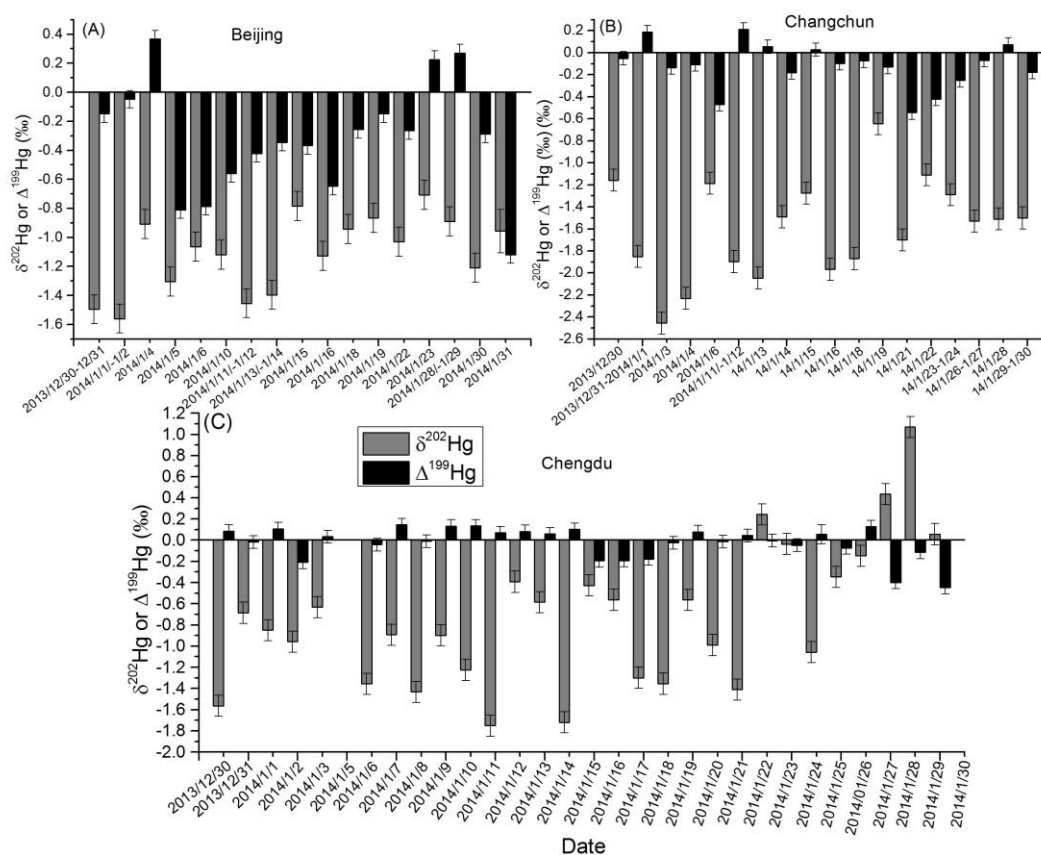


Figure 2. Temporal variations of $\delta^{202}\text{Hg}$ and $\Delta^{199}\text{Hg}$ in studied $\text{PM}_{2.5}$ samples from Beijing (A), Changchun (B) and Chengdu (C).

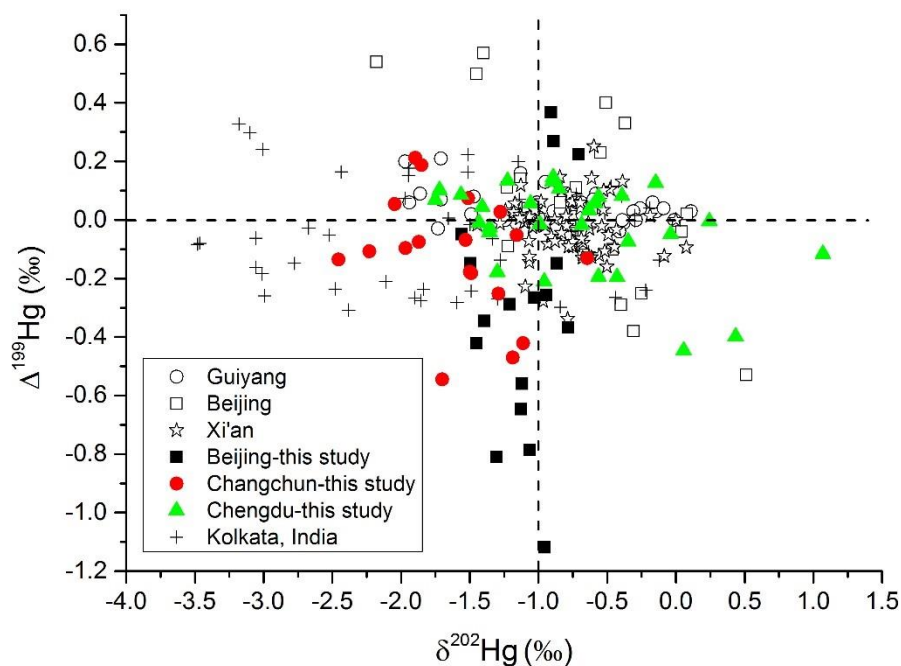


Figure 3. $\delta^{202}\text{Hg}$ vs. $\Delta^{199}\text{Hg}$ in studied $\text{PM}_{2.5}$ samples (■Beijing; ●Changchun; ▲Chengdu) as compared to particulates from previous studies: $\text{PM}_{2.5}$ and TSP from Guiyang (○) (Huang et al., 2015; Yu et al., 2016); $\text{PM}_{2.5}$ from Beijing (□) (Huang et al., 2016); TSP from Xi'an (☆) (Xu et al., 2017b); PM_{10} from Kolkata of India (+) (Das et al., 2016).

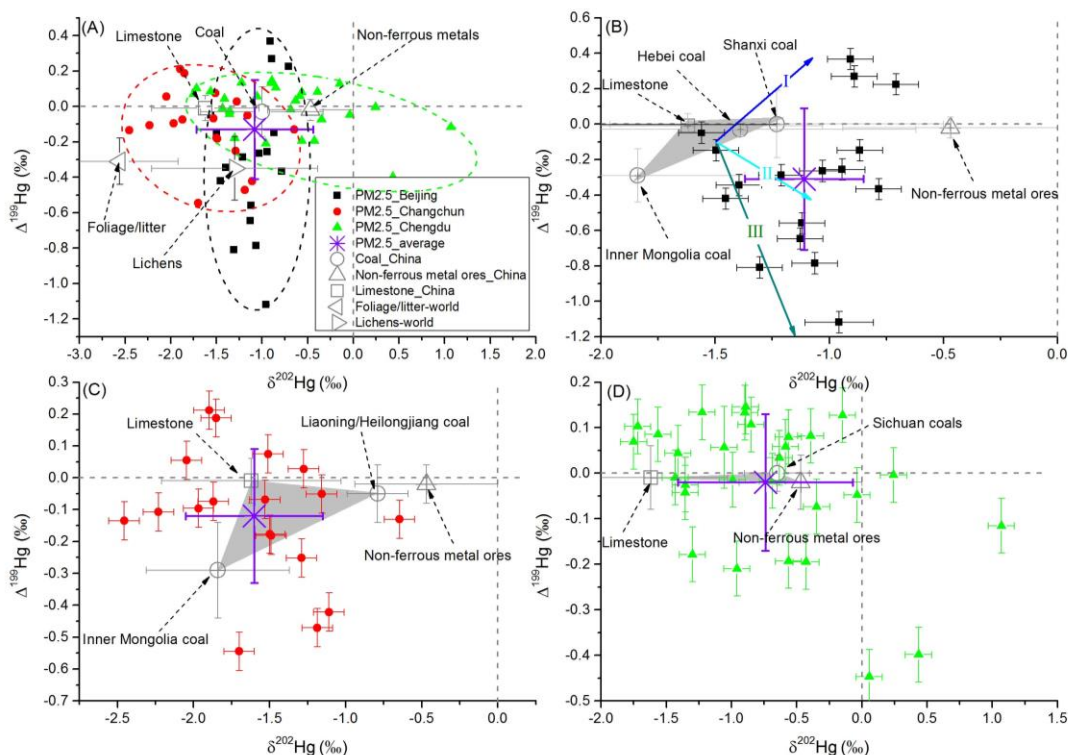


Figure 4. $\delta^{202}\text{Hg}$ vs. $\Delta^{199}\text{Hg}$ in studied $\text{PM}_{2.5}$ samples (■Beijing; ●Changchun; ▲Chengdu) from all three cities (A), Beijing (B), Changchun (C) and Chengdu (D) for source and process identification. The ellipses in (A) are used to outline the variation ranges of $\delta^{202}\text{Hg}$ and $\Delta^{199}\text{Hg}$ in $\text{PM}_{2.5}$ of each city; the shaded areas in (B)-(D) represent the most likely Hg isotope compositions of $\text{PM}_{2.5}$ source materials. The error bars on source materials and $\text{PM}_{2.5}$ -average represent 1σ of sample Hg isotope heterogeneity, and the error bars on $\text{PM}_{2.5}$ samples represent 2σ of Hg isotope analytic uncertainty. The solid arrow trajectories denote different isotope fractionation pathways for Hg^{II} photoreduction.

3.2. Enrichment factor (EF) and elemental correlation

EF of an element is a common geochemical indicator to quantify the crustal versus non-crustal contributions to elemental loadings of aerosols (Cao et al., 2005; Huang et al., 2016), which is calculated by dividing the concentration of interested element in the sample by its abundance in the upper continental crust (UCC) (Rudnick & Gao, 2003) after normalizing to a process-insensitive reference element (e.g. Al, Fe, Ti). Here, we

use Ti as the reference element, and EF of the interested element is written as:

$$EF = [E/Ti]_{\text{sample}} / [E/Ti]_{\text{UCC}} \quad (3)$$

where E is the interested element in the sample. The element is considered to originate mainly from crustal and non-crustal sources, respectively, if EF is 1-5 and >5 (Cao et al., 2005; Huang et al., 2016). Tables S4 and S5 list the volumetric concentrations of elements measured in selected PM_{2.5} samples from the four cities, and the calculated EFs. The mean EF of Hg was 1330 ± 1066 (1σ , $n=10$, 137 to 3302) for Chengdu, 252 ± 192 (1σ , $n=9$, 32 to 565) for Beijing, 158 ± 109 (1σ , $n=10$, 48 to 365) for Changchun and 115 ± 51 (1σ , $n=10$, 54 to 197) for Hong Kong (Tables 1 and S5), indicating that anthropogenic contribution to Hg enrichment in PM_{2.5} was prominent.

High EFs (>100) were also observed for other elements such as S (243 ± 62), Cl (137 ± 113), Cu (145 ± 17), Zn (376 ± 199) and Pb (410 ± 168) (Table S5). Elements including Hg, S, Co, Cr, Pb, Cu, Zn are the major elements released during coal combustion and non-ferrous metal smelting processes (Fang et al., 2014; Pacyna, 1984; Tian et al., 2012; Tian et al., 2014; Ye et al., 2015). Fe ($EF=1.7 \pm 0.1$), Mn ($EF=4.9 \pm 1.0$) and Ca ($EF=1.4 \pm 0.3$) were slightly enriched in the studied PM_{2.5} samples, suggesting their crustal sources, probably from fugitive dusts during cement production (Kong et al., 2011; Tao et al., 2014; Zhang et al., 2005). We found significant correlations between Hg and several elements in Beijing ($r_{Cr-Hg}=0.980$, $r_{Pb-Hg}=0.970$, $r_{Mn-Hg}=0.968$, $r_{Fe-Hg}=0.915$, $r_{S-Hg}=0.887$, $r_{Co-Hg}=0.840$, $r_{Ti-Hg}=0.811$, $r_{Cu-Hg}=0.798$) and Hong Kong ($r_{Mn-Hg}=0.926$, $r_{S-Hg}=0.818$, $r_{Cr-Hg}=0.803$, $r_{Cu-Hg}=0.803$, $r_{Fe-Hg}=0.779$, $r_{K-Hg}=0.775$, $r_{Ti-Hg}=0.773$, $r_{Zn-Hg}=0.766$) (Table S6). However, no significant correlations were observed between Hg and other elements in Changchun and Chengdu (Table S6). This suggests again that the factors controlling Hg enrichment in PM_{2.5} are more complex in Changchun and Chengdu than Beijing and Hong Kong.

3.3. Potential Hg sources of PM_{2.5} in Chinese cities

A recent comprehensive study showed that coal combustion (47%) is the primary source of atmospheric Hg in China, followed by equal contributions from cement

production (18%) and non-ferrous metal (Pb, Cu, Zn) smelting (18%) (Zhang et al., 2015). It is noted that the contributions of these sources might differ significantly in different provinces or regions. For example, the dominant atmospheric Hg contributors in Jilin Province (whose capital is Changchun) are coal combustion and cement production, and in Hebei Province (bordering to Beijing) are coal combustion, cement production, and iron and steel production.

Overall, the PM_{2.5} samples were characterized by moderately negative $\delta^{202}\text{Hg}$ ($-1.08\pm 0.64\text{‰}$, 1σ , $n=64$) and slightly negative $\Delta^{199}\text{Hg}$ ($-0.13\pm 0.28\text{‰}$, 1σ , $n=64$) (Table S3). No significant MIF for even Hg isotopes ($\Delta^{200}\text{Hg}=0.03\pm 0.05\text{‰}$; $\Delta^{204}\text{Hg}=-0.04\pm 0.14\text{‰}$, 1σ , $n=64$) was observed, which is consistent with the insignificant $\Delta^{200}\text{Hg}$ values of anthropogenic Hg emissions (Sun et al., 2016c). The mean values of $\delta^{202}\text{Hg}$ for coals (Biswas et al., 2008; Sun et al., 2013b; Sun et al., 2014a; Sun et al., 2014b; Yin et al., 2014a), non-ferrous metal ores (Yin et al., 2016) and limestone (used for cement production) (Sun et al., 2016c) in China are $-1.00\pm 0.67\text{‰}$, $-0.47\pm 0.77\text{‰}$ and $-1.62\pm 0.59\text{‰}$ (1σ), respectively, which overlap the middle region of $\delta^{202}\text{Hg}$ values of collected PM_{2.5} samples (Figure 4A). However, the $\Delta^{199}\text{Hg}$ variation range of PM_{2.5} samples (-1.13‰ to 0.37‰) is much larger than those of the above and other anthropogenic source materials that are commonly characterized by circum-zero $\Delta^{199}\text{Hg}$ values varying between -0.15‰ and 0.15‰ (Sun et al., 2016c). Biomass including forest foliage/litter and lichen (Carignan et al., 2009; Demers et al., 2013; Enrico et al., 2016; Jiskra et al., 2015; Wang et al., 2017; Yu et al., 2016; Zhang et al., 2013; Zheng et al., 2016) is characterized by large negative $\Delta^{199}\text{Hg}$ value, down to -1.0‰ (Figure 4A), and biomass burning could be an important contributor of PM_{2.5}-bound Hg (Huang et al., 2016). However, we found no strong correlation between $\Delta^{199}\text{Hg}$ and K^+ concentration indicative of biomass burning influence (Andreae, 1983). The days for fire occurrences surrounding the studied cities did not correspond well to PM_{2.5} samples of large negative $\Delta^{199}\text{Hg}$ values (Table S7). Further, previous studies have demonstrated that industrial or combustion processing of source materials can only cause MDF, rather than MIF (see discussion in section 3.4) (Sonke et al., 2010;

Sun et al., 2013b; Sun et al., 2014a; Wiederhold et al., 2013; Yin et al., 2013). Thus, the observed Hg isotope compositions of all PM_{2.5} samples could not be fully explained by source contribution and Hg isotope fractionation during emission processes. From the near-unity slope (0.98) of $\Delta^{199}\text{Hg}$ vs. $\Delta^{201}\text{Hg}$ in the PM_{2.5} samples (Figure 5), we suggest that Hg^{II} photoreduction was a critical factor to result in the observed Hg isotope compositions (Bergquist and Blum, 2007; Das et al., 2016; Huang et al., 2016; Rolison et al., 2013).

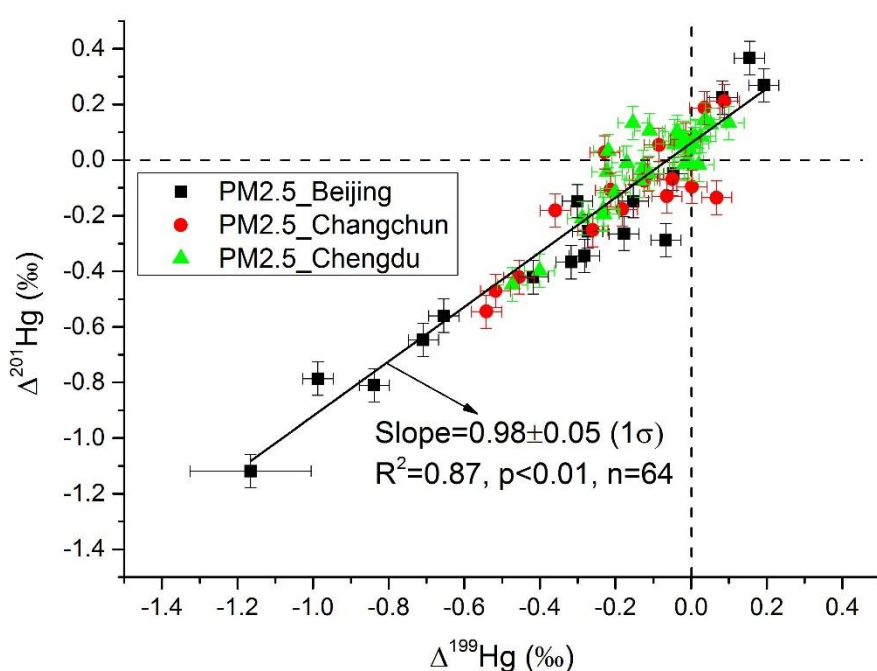


Figure 5. Linear regression of $\Delta^{199}\text{Hg}$ vs. $\Delta^{201}\text{Hg}$ in studied PM_{2.5} samples (■Beijing; ●Changchun; ▲Chengdu) from China.

3.3.1. PM_{2.5} in Beijing

PM_{2.5} samples collected in Beijing had a limited variation in $\delta^{202}\text{Hg}$ (-1.56‰ to -0.71‰) and a large variation in $\Delta^{199}\text{Hg}$ (-1.12‰ to 0.37‰) (Figures 2A and 4B). $\delta^{202}\text{Hg}$ values of PM_{2.5} samples only partly overlapped the typical $\delta^{202}\text{Hg}$ variation ranges of the combusted coals in Beijing (imported from Shanxi and Hebei Province) and adjacent Hebei Province (mostly imported from Inner Mongolia and Shanxi Province), limestone and non-ferrous metal ores (Sun et al., 2016b; Sun et al., 2016c; Yin et al.,

2016; Zhang et al., 2015). On average, $\delta^{202}\text{Hg}$ value of $\text{PM}_{2.5}$ samples was higher than those of coals (combusted in Beijing and Hebei Province) and limestone by 0.1‰-0.7‰, but was lower than that of non-ferrous metal ores by ~0.6‰. About half of $\text{PM}_{2.5}$ samples had $\Delta^{199}\text{Hg}$ values above 0.2‰ or below -0.4‰, significantly exceeding the $\Delta^{199}\text{Hg}$ ranges of these potential source materials and biomass. As suggested by the near-unity slope of $\Delta^{199}\text{Hg}$ vs. $\Delta^{201}\text{Hg}$ ($\Delta^{199}\text{Hg}=0.96\times\Delta^{201}\text{Hg}+0.02$, $R^2=0.92$, $n=17$), a certain fraction of $\text{PM}_{2.5}$ -bound Hg was likely photochemically reduced before sample collection.

Photochemical reduction of Hg^{II} can result in distinct Hg isotope fractionation trajectories (Blum et al., 2014). Photoreduction of Hg^{II} bound to dissolved organic matter and non-sulfur ligands has been demonstrated to produce a positive $\Delta^{199}\text{Hg}/\delta^{202}\text{Hg}$ slope (Bergquist and Blum, 2007; Zheng and Hintelmann, 2010), with a value of around 1.2 (Type I), whereas photoreduction of Hg^{II} bound to sulfur-containing ligands produces a negative $\Delta^{199}\text{Hg}/\delta^{202}\text{Hg}$ slope of around -0.8 (Type II) (Zheng and Hintelmann, 2010). A negative $\Delta^{199}\text{Hg}/\delta^{202}\text{Hg}$ slope as low as -3.5 has been observed during photoreduction of Hg^{II} from snow crystals (Type III) (Sherman et al., 2010). Because all these types of Hg^{II} photoreduction enrich heavier Hg isotopes in the residual Hg^{II} , the $\delta^{202}\text{Hg}$ values of $\text{PM}_{2.5}$ source materials are supposed to be lower than those of collected $\text{PM}_{2.5}$ samples. Thus, the most likely Hg source materials are coal and limestone rather than non-ferrous metal ores. This is in consistence with the bottom-up Hg emission inventory estimated by Zhang et al. (2015) for Hebei Province and Beijing where Hg emission budget from non-ferrous metal smelting is much less than that of coal combustion or cement production. In addition, some typical coal combustion pollutants such as SO_2 , CO and NO_2 are all well correlated with $\text{Hg}_{\text{PM}_{2.5}}$ in Beijing (Table S8).

Shown in Figure 4B are three potential Hg isotope fractionation trajectories of photoreduction with an assumed starting source Hg isotope composition of -1.5‰ for $\delta^{202}\text{Hg}$ and -0.1‰ for $\Delta^{199}\text{Hg}$ (similar to the mean Hg isotope compositions of combusted coals and limestone). The three Hg isotope fractionation trajectories can

broadly reproduce the observed $\Delta^{199}\text{Hg}$ ranges of $\text{PM}_{2.5}$ in Beijing (-1.1‰ to 0.4‰) when $\delta^{202}\text{Hg}$ increases from -1.5‰ (assumed starting source materials) to -1.1‰ (mean of the collected $\text{PM}_{2.5}$ samples). Although the Type III photoreductive pathway typically for arctic snow crystals could reproduce the large negative $\Delta^{199}\text{Hg}$ values in some $\text{PM}_{2.5}$ samples, it unlikely occurred in urban fine aerosols. Huang et al. (2016) suggested that biomass burning surrounding Beijing possibly imparted the fine aerosols with negative $\Delta^{199}\text{Hg}$ between -0.5‰ and -0.3‰. A recent study showed high contribution of biomass burning to the fine aerosols in Beijing around 2013-2014 (Zhang et al., 2017), which might explain these large negative $\Delta^{199}\text{Hg}$ values of collected $\text{PM}_{2.5}$ samples. However, we did not observe a good coincidence of low $\Delta^{199}\text{Hg}$, high K^+ concentrations in the fire occurrence days (Table S7). The $\text{PM}_{2.5}$ sample collected in the first day of Chinese New Year (31/01/2014) has the most negative $\Delta^{199}\text{Hg}$ value (-1.1‰) and highest Hg concentration ($6.38 \mu\text{g g}^{-1}$), likely relating to the intensive burning of fireworks (Ji et al., 2018; Thakur et al., 2010). Therefore, we suggest that the large spread of $\Delta^{199}\text{Hg}$ and high $\delta^{202}\text{Hg}$ (relative to source materials) in $\text{PM}_{2.5}$ samples from Beijing was mainly attributed to isotope fractionation via photoreductive pathways of aerosol Hg^{II} .

3.3.2. $\text{PM}_{2.5}$ in Changchun

$\text{PM}_{2.5}$ samples collected in Changchun were characterized by the most negative $\delta^{202}\text{Hg}$ (-2.46‰ to -0.65‰) and small negative to positive $\Delta^{199}\text{Hg}$ (-0.54‰ to 0.21‰) (Figures 2B and 4C), which largely overlapped with the those of combusted coals in Jilin Province (partly imported from Inner Mongolia and two neighboring provinces, Heilongjiang and Liaoning) and limestone, rather than non-ferrous metal ores (Sun et al., 2016b; Sun et al., 2016c; Yin et al., 2016; Zhang et al., 2015). This likely suggests that coal combustion and cement production were the primary sources of Hg in $\text{PM}_{2.5}$ samples from Changchun, consistent with the estimated primary Hg emission source for Jilin Province by Zhang et al. (2015). Only several $\text{PM}_{2.5}$ samples had $\Delta^{199}\text{Hg}$ values that exceeded the mean $\pm 1\sigma$ ranges of $\Delta^{199}\text{Hg}$ of these potential source materials (Figure 4C). We found that the samples with $\Delta^{199}\text{Hg}$ values below -0.15‰ generally had high K^+ concentrations and coincided with fire occurrence time near the sample

collection days (e.g. 14/01/2014, 21/01/2014-24/01/2014, 29/01/2014-30/01/2014) (Table S7), suggesting biomass burning as an additional Hg source. The slope of $\Delta^{199}\text{Hg}$ vs. $\Delta^{201}\text{Hg}$ ($\Delta^{199}\text{Hg}=0.91\times\Delta^{201}\text{Hg}+0.03$, $R^2 = 0.73$, $n=18$) is near unity, indicating the MIF in $\text{PM}_{2.5}$ was imparted by photochemical reduction of Hg^{II} . However, the possible biomass burning contribution and small $\Delta^{199}\text{Hg}$ anomalies in most samples suggest that the aerosol Hg^{II} photoreduction in Changchun was not as evident as that in Beijing. It is noted that the sunlight duration between Changchun and Beijing during the sampling period was comparable (198 h vs. 192 h), suggesting sunlight duration is not the only factor controlling the extent of aerosol Hg^{II} photoreduction. We also noted that the temperature of Changchun was much lower than that in Beijing ($-14.2\text{ }^{\circ}\text{C}$ vs. $-0.8\text{ }^{\circ}\text{C}$), implying that lower temperature might suppress the aerosol Hg^{II} photoreduction. The above speculation is consistent with previous studies which demonstrated that elemental Hg volatilization from soil pool can be enhanced with the increase of solar radiation duration and temperature (Gustin et al., 2002; Lindberg et al., 1995).

3.3.3. $\text{PM}_{2.5}$ in Chengdu

$\text{PM}_{2.5}$ samples collected in Chengdu were characterized by the most positive $\delta^{202}\text{Hg}$ (-1.75‰ to 1.07‰) and small values of $\Delta^{199}\text{Hg}$ (-0.21‰ to 0.15‰ for 27 out of 29 samples) (Figures 2C and 4D). The combusted coals (mostly self-production) of Sichuan, limestone and non-ferrous metal ores (Sun et al., 2016b; Sun et al., 2016c; Yin et al., 2016; Zhang et al., 2015) overlapped with most of the $\text{PM}_{2.5}$ samples within uncertainty, suggesting these materials were the potential Hg sources of $\text{PM}_{2.5}$ from Chengdu. Zhang et al. (2015) estimated that coal combustion, cement production and non-ferrous metal smelting are the largest three atmospheric Hg contributors in Sichuan Province. The most negative $\Delta^{199}\text{Hg}$ values were observed in samples collected from 26/01/2014 (-0.40‰) and 28/01/2014 (-0.45‰), the periods when high frequency of fires were detected surrounding the Chengdu city (Table S7). This suggests again biomass burning as an additional Hg source in specific days. The slope of $\Delta^{199}\text{Hg}$ vs. $\Delta^{201}\text{Hg}$ ($\Delta^{199}\text{Hg}=0.96\times\Delta^{201}\text{Hg}+0.08$, $R^2=0.76$, $n=29$) in $\text{PM}_{2.5}$ samples from Chengdu is also near unity. As compared to Beijing and Changchun, Chengdu had two times less

sunlight duration (Table S1). The limited $\Delta^{199}\text{Hg}$ anomalies of most samples in Chengdu possibly indicate that the aerosol Hg^{II} photoreduction was negligible.

3.4. Possible isotope fractionation before and after Hg emissions

The industrial processing of source materials may induce significant MDF, causing large shifts in $\delta^{202}\text{Hg}$ values of emitted Hg species relative to the source materials (Sonke et al., 2010; Sun et al., 2013b; Sun et al., 2014a; Wiederhold et al., 2013; Yin et al., 2013). However, the signs and magnitudes of Hg isotope fractionation within the emission sources are not well understood except for coal combustion in the coal-fired utility boilers (Sun et al., 2016c). Sun et al. (2013b) showed that the fly ash (representing PBM) generated by the boilers equipped with electrostatic precipitators (ESPs) and wet flue gas desulfurization (WFGD) was enriched in lighter Hg isotopes by $\sim 0.8\text{‰}$ in $\delta^{202}\text{Hg}$ relative to the source coals. Subsequently, Tang et al. (2017) showed that the fly ash generated by boilers equipped with ESP+WFGD and additional selective catalytic reduction system (SCR) was only slightly enriched in lighter Hg isotopes ($\sim 0.2\text{‰}$ in $\delta^{202}\text{Hg}$) relative to the source coals. In contrast, Sun et al. (2016c) suggested that the emitted Hg species during cement production and non-ferrous metal smelting conserve the Hg isotope compositions of limestone and non-ferrous metal ores, respectively. More than 80% of coal-fired utility boilers are installed with SCR in Beijing (Zhang et al., 2012), it is thus expected that the emitted fly ash is very similar to the combusted coals in $\delta^{202}\text{Hg}$. However, the coal-fired utility boilers in Jilin province and Sichuan province are only installed with ESPs or ESP+WFGD (Zhang et al., 2012), the emitted fly ash is likely lower in $\delta^{202}\text{Hg}$ than the combusted coals. The lower $\delta^{202}\text{Hg}$ values of $\text{PM}_{2.5}$ samples in Changchun than Beijing probably (Table 1) implies significant MDF within coal-fired utility boilers from Jilin province.

Following Hg emission to the atmosphere, the atmospheric processes may transform emitted GEM, GOM and PBM, which potentially fractionates Hg isotopes as well. An experimental study showed that GEM oxidation could cause significant MDF and MIF, resulting in a characteristic $\Delta^{199}\text{Hg}/\Delta^{201}\text{Hg}$ slope of 1.6 for Br-initiated

oxidation and 1.9 for Cl-initiated oxidation (Sun et al., 2016a). Both slopes are significantly higher than that (~ 1) of $\Delta^{199}\text{Hg}/\Delta^{201}\text{Hg}$ in our $\text{PM}_{2.5}$ samples, suggesting that $\text{PM}_{2.5}$ -bound Hg unlikely derived from halogen-assisted GEM oxidation. However, $\text{PM}_{2.5}$ -bound Hg might contain GEM and GOM adsorbed onto the fine particulates. Both empirical models and in-situ measurement of coal-fired utility boilers indicated that the GEM and GOM generated from coal combustion have higher $\delta^{202}\text{Hg}$ than PBM (Sun et al., 2013b; Tang et al., 2017). However, isotope fractionation of emitted Hg species in other anthropogenic sources is largely unknown. Considering the fractions of GEM and GOM adsorbed onto the collected $\text{PM}_{2.5}$ are commonly small (Fu et al., 2016b), we suggest that the influence of gaseous Hg adsorption on the observed Hg isotope compositions is negligible.

4. Conclusions

In this study, 24 h-integrated $\text{PM}_{2.5}$ samples were collected from four large Chinese cities (Beijing, Changchun, Chengdu and Hong Kong) in the January 2014 when the haze pollution levels were the highest in mainland China. By coupling with source indicator elements and climate conditions, we suggest that the Hg isotope compositions of our collected $\text{PM}_{2.5}$ samples are the best explained by Hg contributions from the dominant anthropogenic sources (coal combustion and cement production, with additional non-ferrous metal smelting for Chengdu), superimposed by biomass burning on specific days. The aerosol Hg^{II} photoreduction in Beijing potentially fractionated Hg isotopes along different trajectories, significantly shifting the Hg isotope compositions of contributing sources of $\text{PM}_{2.5}$. Notably, the distinguishability in Hg isotope compositions of $\text{PM}_{2.5}$ samples between the studied Chinese capital cities (Figure 4A) would be useful for tracing the regional inflows and outflows of $\text{PM}_{2.5}$ and $\text{PM}_{2.5}$ bound Hg.

Acknowledgements

This work was supported by the National Natural Science Foundation of China

(41503096; 41773104) and the National Key Research and Development Plan (2016YFC0201600; 2017YFC0212700). Supports from the Chinese Government Scholarship (CSC No. 201506285035) and open fund by State Key Laboratory of Loess and Quaternary Geology, Institute of Earth Environment, CAS (SKLLQG1722) are also thanked.

Author contribution

H.X. and R.S. conceived and designed this study. H.X., M.J., C.L., B.D., S.L. and T.Z. carried out the particulate samples collection and experiments. H.X., R.S. and J.S. processed the experimental data. H.X. and R.S. contributed to the literature search, data analysis and interpretation, and manuscript writing. J.C., R.H., J.S., B.G., Z.S. and C.H. contributed to manuscript revision. All authors reviewed the manuscript.

Conflict of interest

The authors declare that they have no conflict of interest.

References

- Amos, H.M. et al., 2012. Gas-particle partitioning of atmospheric Hg(II) and its effect on global mercury deposition. *Atmos. Chem. Phys.*, 12: 591-603.
- Andreae, M.O., 1983. Soot carbon and excess fine potassium: long-range transport of combustion-derived aerosols. *Science*, 220: 1148-1151.
- Bergquist, B.A., Blum, J.D., 2007. Mass-dependent and -independent fractionation of Hg isotopes by photoreduction in aquatic systems. *Science*, 318: 417-420.
- Biswas, A. et al., 2008. Natural mercury isotope variation in coal deposits and organic soils. *Environ. Sci. Technol.*, 42: 8303-8309.
- Blum, J.D. et al., 2014. Mercury isotopes in earth and environmental sciences. *Annu. Rev. Earth Pl. Sc.*, 42: 249-269.
- Cao, J.J. et al., 2013. Evolution of PM_{2.5} measurements and standards in the U.S. and future perspectives for China. *Aerosol Air Qual. Res.*, 13: 1197-1211.
- Cao, J.J. et al., 2012. Fine particulate matter constituents and cardiopulmonary mortality in a heavily polluted Chinese city. *Environ. Health Perspect.*, 120: 373-378.
- Cao, J.J. et al., 2005. Composition of indoor aerosols at emperor Qin's terra-cotta museum, Xi'an, China, during summer, 2004. *Particuology*, 3: 170-175.
- Carignan, J. et al., 2009. Odd isotope deficits in atmospheric Hg measured in lichens. *Environ. Sci.*

- Technol., 43: 5660-5664.
- Chen, J. et al., 2012. Unusual fractionation of both odd and even mercury isotopes in precipitation from Peterborough, ON, Canada. *Geochim. Cosmochim. Ac.*, 90: 33-46.
- Das, R. et al., 2016. Mercury isotopes of atmospheric particle bound mercury for source apportionment study in urban Kolkata, India. *Elementa: Science of the Anthropocene*, 4: 000098.
- Demers, J.D. et al., 2013. Mercury isotopes in a forested ecosystem: Implications for air-surface exchange dynamics and the global mercury cycle. *Global Biogeochem. Cy.*, 27: 222-238.
- Demers, J.D. et al., 2015. Coupling atmospheric mercury isotope ratios and meteorology to identify sources of mercury impacting a coastal urban-industrial region near Pensacola, Florida, USA. *Global Biogeochem. Cy.*, 29: 1689-1705.
- Dockery, D., Pope, A., 1996. Epidemiology of acute health effects: summary of time-series studies, In: Wilson, R., Spengler, J.D. (Eds.). *Particles in Air: Concentration and Health Effects*, University Press, Cambridge, USA.
- Donovan, P.M. et al., 2013. An isotopic record of mercury in San Francisco Bay sediment. *Chem. Geol.*, 349-350: 87-98.
- Driscoll, C.T. et al., 2013. Mercury as a global pollutant: Sources, pathways, and effects. *Environ. Sci. Technol.*, 47: 4967-4983.
- Enrico, M. et al., 2016. Atmospheric mercury transfer to peat bogs dominated by gaseous elemental mercury dry deposition. *Environ. Sci. Technol.*, 50: 2405-2412.
- Fang, T. et al., 2014. Lead in Chinese coals: Distribution, modes of occurrence, and environmental effects. *Environ. Geochem. Hlth.*, 36: 563-581.
- Fu, X. et al., 2016a. Isotopic composition of gaseous elemental mercury in the free Troposphere of the Pic du Midi Observatory, France. *Environ. Sci. Technol.*, 50: 5641-5650.
- Fu, X. et al., 2015. Observations of atmospheric mercury in China: A critical review. *Atmos. Chem. Phys.*, 15: 9455-9476.
- Fu, X. et al., 2016b. Atmospheric wet and litterfall mercury deposition at urban and rural sites in China. *Atmos. Chem. Phys.*, 16: 11547-11562.
- GB3095-2012, 2012. Ambient air quality standards. Ministry of environmental protection and general administration of quality supervision. Inspection and Quarantine of the People's Republic of China.
- Gratz, L.E. et al., 2010. Isotopic composition and fractionation of mercury in Great Lakes precipitation and ambient air. *Environ. Sci. Technol.*, 44: 7764-7770.
- Gustin, M.S. et al., 2002. Investigation of the light-enhanced emission of mercury from naturally enriched substrates. *Atmos. Environ.*, 36(20): 3241-3254.
- Gustin, M.S. et al., 2015. Measuring and modeling mercury in the atmosphere: A critical review. *Atmos. Chem. Phys.*, 15: 5697-5713.
- Ho, K.F. et al., 2003. Characterization of chemical species in PM_{2.5} and PM₁₀ aerosols in Hong Kong. *Atmos. Environ.*, 37: 31-39.
- Horowitz, H.M. et al., 2017. A new mechanism for atmospheric mercury redox atmospheric chemistry and physics: implications for the global mercury budget. *Atmos. Chem. Phys.*, 17: 6353-6371.
- Huang, Q. et al., 2016. Isotopic composition for source identification of mercury in atmospheric fine particles. *Atmos. Chem. Phys.*, 16: 11773-11786.
- Huang, Q. et al., 2015. An improved dual-stage protocol to pre-concentrate mercury from airborne

- particles for precise isotopic measurement. *J. Anal. Atom. Spectrom.*, 30: 957-966.
- Huang, R.-J. et al., 2014. High secondary aerosol contribution to particulate pollution during haze events in China. *Nature*, 514: 218-222.
- Jahn, H.J. et al., 2011. Particulate matter pollution in the megacities of the Pearl River Delta, China – A systematic literature review and health risk assessment. *Int. J. Hyg. Envir. Heal.*, 214: 281-295.
- Ji, D.S. et al., 2018. Characterization and source identification of fine particulate matter in urban Beijing during the 2015 Spring Festival. *Sci. Total Environ.*, 628-629: 430-440.
- Jiskra, M. et al., 2015. Mercury deposition and re-emission pathways in boreal forest soils investigated with Hg isotope signatures. *Environ. Sci. Technol.*, 49: 7188-7196.
- Kong, S. et al., 2011. Characterization of PM₁₀ source profiles for fugitive dust in Fushun-a city famous for coal. *Atmos. Environ.*, 45: 5351-5365.
- Lindberg, S.E. et al., 1995. Micrometeorological gradient approach for quantifying air/surface exchange of mercury vapor: tests over contaminated soils. *Environ. Sci. Technol.*, 29(1): 126-135.
- Pacyna, J.M., 1984. Estimation of the atmospheric emissions of trace elements from anthropogenic sources in Europe. *Atmos. Environ.*, 18: 41-50.
- Rolison, J.M. et al., 2013. Isotopic composition of species-specific atmospheric Hg in a coastal environment. *Chem. Geol.*, 336: 37-49.
- Rudnick, R., Gao, S., 2003. Composition of the continental crust, *Treatise on Geochemistry*, 3: 1-64.
- Selin, N.E. et al., 2007. Chemical cycling and deposition of atmospheric mercury: Global constraints from observations. *J. Geophys. Res.*, 112(D2): D02308.
- Sherman, L.S. et al., 2015. The use of Pb, Sr, and Hg isotopes in Great Lakes precipitation as a tool for pollution source attribution. *Sci. Total Environ.*, 502: 362-374.
- Sherman, L.S. et al., 2010. Mass-independent fractionation of mercury isotopes in Arctic snow driven by sunlight. *Nat. Geosci.*, 3: 173-177.
- Sherman, L.S. et al., 2012. Investigation of local mercury deposition from a coal-fired power plant using mercury isotopes. *Environ. Sci. Technol.*, 46: 382-390.
- Smith, R.S. et al., 2015. Mercury isotope fractionation during precipitation of metacinnabar (β -HgS) and montroydite (HgO). *Environ. Sci. Technol.*, 49: 4325-4334.
- Sonke, J.E., Blum, J.D., 2013. Advances in mercury stable isotope biogeochemistry. *Chem. Geol.*, 336: 1-4.
- Sonke, J.E. et al., 2010. Sedimentary mercury stable isotope records of atmospheric and riverine pollution from two major European heavy metal refineries. *Chem. Geol.*, 279: 90-100.
- Sun, G. et al., 2016a. Mass-dependent and -independent fractionation of mercury isotope during gas-phase oxidation of elemental mercury vapor by atomic Cl and Br. *Environ. Sci. Technol.*, 50: 9232-9241.
- Sun, R. et al., 2013a. A double-stage tube furnace-acid-trapping protocol for the pre-concentration of mercury from solid samples for isotopic analysis. *Anal. Bioanal. Chem.*, 405: 6771-6781.
- Sun, R. et al., 2013b. Mercury stable isotope fractionation in six utility boilers of two large coal-fired power plants. *Chem. Geol.*, 336: 103-111.
- Sun, R. et al., 2014a. Mercury stable isotope signatures of world coal deposits and historical coal combustion emissions. *Environ. Sci. Technol.*, 48: 7660-7668.
- Sun, R. et al., 2016b. Biogeochemical controls on mercury stable isotope compositions of world coal deposits: A review. *Earth-Sci. Rev.*, 152: 1-13.
- Sun, R. et al., 2014b. Variations in the stable isotope composition of mercury in coal-bearing sequences:

- Indications for its provenance and geochemical processes. *Int. J. Coal Geol.*, 133: 13-23.
- Sun, R. et al., 2016c. Historical (1850-2010) mercury stable isotope inventory from anthropogenic sources to the atmosphere. *Elementa: Science of the Anthropocene*, 4: 000091.
- Tang, S. et al., 2017. Stable isotope composition of mercury forms in flue gases from a typical coal-fired power plant, Inner Mongolia, northern China. *J. Hazard. Mater.*, 328: 90-97.
- Tao, J. et al., 2014. PM_{2.5} pollution in a megacity of southwest China: Source apportionment and implication. *Atmos. Chem. Phys.*, 14: 8679-8699.
- Thakur, B. et al., 2010. Air pollution from fireworks during festival of lights (Deepawali) in Howrah, India - a case study. *Atmósfera*, 23(4): 347-365.
- Tian, H. et al., 2012. Temporal and spatial variation characteristics of atmospheric emissions of Cd, Cr, and Pb from coal in China. *Atmos. Environ.*, 50: 157-163.
- Tian, H. et al., 2014. Atmospheric emission inventory of hazardous trace elements from China's coal-fired power plants-temporal trends and spatial variation characteristics. *Environ. Sci. Technol.*, 48: 3575-3582.
- USEPA, 2006. Special Report on Lead Pollution. U.S. Environmental Protective Agency.
- Wang, Z. et al., 2015. Mass-dependent and mass-independent fractionation of mercury isotopes in precipitation from Guiyang, SW China. *C.R. Geosci.*, 347: 358-367.
- Wang, X. et al., 2017. Using mercury isotopes to understand mercury accumulation in the montane forest floor of the Eastern Tibetan Plateau. *Environ. Sci. Technol.*, 51: 801-809.
- WHO, 2007. World Health Organization, Exposure to mercury: A major public health concern. WHO, Public Health and Environment, L Geneva.
- Wiederhold, J.G. et al., 2013. Mercury isotope signatures as tracers for Hg cycling at the New Idria Hg mine. *Environ. Sci. Technol.*, 47: 6137-6145.
- Xu, H.M. et al., 2016. Inter-annual variability of wintertime PM_{2.5} chemical composition in Xi'an, China: Evidences of changing source emissions. *Sci. Total Environ.*, 545-546: 546-555.
- Xu, H.M. et al., 2012. Lead concentrations in fine particulate matter after the phasing out of leaded gasoline in Xi'an, China. *Atmos. Environ.*, 46: 217-224.
- Xu, H. et al., 2017a. A 10-year observation of PM_{2.5}-bound nickel in Xi'an, China: Effects of source control on its trend and associated health risks. *Sci. Rep.*, 7: 41132.
- Xu, H. et al., 2017b. Seasonal and annual variations in atmospheric Hg and Pb isotopes in Xi'an, China. *Environ. Sci. Technol.*, 51: 3759-3766.
- Ye, X. et al., 2015. Atmospheric mercury emissions from China's primary nonferrous metal (Zn, Pb and Cu) smelting during 1949-2010. *Atmos. Environ.*, 103: 331-338.
- Yin, R. et al., 2014a. Mercury stable isotopic compositions in coals from major coal producing fields in China and their geochemical and environmental implications. *Environ. Sci. Technol.*, 48: 5565-5574.
- Yin, R. et al., 2016. Mercury isotopes as proxies to identify sources and environmental impacts of mercury in Sphalerites. *Sci. Rep.*, 6: 18686.
- Yin, R. et al., 2014b. Trends and advances in mercury stable isotopes as a geochemical tracer. *Trends Environ. Anal. Chem.*, 2: 1-10.
- Yin, R. et al., 2013. Mercury speciation and mercury isotope fractionation during ore roasting process and their implication to source identification of downstream sediment in the Wanshan mercury mining area, SW China. *Chem. Geol.*, 336: 72-79.
- Yu, B. et al., 2016. Isotopic composition of atmospheric mercury in China: New evidence for source and

- transformation processes in air and in vegetation. *Environ. Sci. Technol.*, 50: 9262-9269.
- Yuan, S. et al., 2015. Large variation of mercury isotope composition during a single precipitation event at Lhasa city, Tibetan Plateau, China. *Procedia Earth Planet. Sci.*, 13: 282-286.
- Zhang, Y. et al., 2017. High contribution of nonfossil sources to submicrometer organic aerosols in Beijing, China. *Environ. Sci. Technol.*, 51: 7842-7852.
- Zhang, D. et al., 2005. Anthropogenic calcium particles observed in Beijing and Qingdao, China. *Water Air Soil Pollut.*, 5: 261-276.
- Zhang, L. et al., 2012. Influence of mercury and chlorine content of coal on mercury emissions from coal-fired power plants in China. *Environ. Sci. Technol.*, 46: 6385-6392.
- Zhang, L. et al., 2015. Updated emission inventories for speciated atmospheric mercury from anthropogenic sources in China. *Environ. Sci. Technol.*, 49: 3185-3194.
- Zhang, H. et al., 2013. Atmospheric mercury inputs in montane soils increase with elevation: evidence from mercury isotope signatures. *Sci. Rep.*, 3: 3322.
- Zhang, T. et al., 2011. Water-soluble ions in atmospheric aerosols measured in Xi'an, China: Seasonal variations and sources. *Atmos. Res.*, 102: 110-119.
- Zheng, W., Hintelmann, H., 2010. Isotope fractionation of mercury during its photochemical reduction by low-molecular-weight organic compounds. *J. Phys. Chem. A*, 114: 4246-4253.
- Zheng, W. et al., 2016. Mercury isotope compositions across North American forests. *Global Biogeochem. Cycles*, 30: 1475-1492.